### Title

Post-contrast myocardial T1 and ECV disagree in a longitudinal canine study




### Journal

NMR in Biomedicine, 27(8)

### ISSN

0952-3480



### Authors

Koopmann, Matthias
Hong, KyungPyo
Kholmovski, Eugene G
et al.



### Publication Date

2014-08-01

### DOI

10.1002/nbm.3135

Peer reviewed

Published in final edited form as:
*NMR Biomed*. 2014 August ; 27(8): 988–995. doi:10.1002/nbm.3135.

# Post-Contrast Myocardial $T_1$ and ECV Disagree in a Longitudinal Canine Study

**Matthias Koopmann, MD**[1,*], **Kyung Pyo Hong, MS**[2,*], **Eugene G. Kholmovski, PhD**[2], **Eric C. Huang, MD, PhD**[3], **Nan Hu, PhD**[4], **Jian Ying, PhD**[4], **Richard Levenson, MD**[3], **Sathya Vijayakumar, MS, MBA**[5], **Derek J. Dosdall, PhD**[6], **Ravi Ranjan, MD, PhD**[6], and **Daniel Kim, PhD**[2]

[1]Division of Electrophysiology, Department of Cardiovascular Medicine, University Hospital of Münster, Münster, Germany

[2]UCAIR, Department of Radiology, University of Utah, Salt Lake City, UT, 84108

[3]Department of Pathology and Laboratory Medicine, University of California, Davis Medical Center, Sacramento, CA, 95817

[4]Division of Epidemiology, Internal Medicine, University of Utah, Salt Lake City, UT, 84112

[5]Surgical Services Clinical Program, Intermountain Healthcare, Salt Lake City, UT, 84111

[6]Division of Cardiology, Internal Medicine, University of Utah, Salt Lake City, UT, 84112

## Abstract

Both post-contrast myocardial $T_1$ and extracellular volume (ECV) measurements have been associated with interstitial fibrosis. The cardiovascular magnetic resonance (CMR) field is migrating towards ECV, because it is largely insensitive to confounders that affect post-contrast myocardial $T_1$. Despite the theoretical advantages of myocardial ECV over post-contrast myocardial $T_1$, systematic experimental studies comparing the two measurements are largely lacking. We sought to measure the temporal changes in post-contrast myocardial $T_1$ and ECV in an established canine model with chronic atrial fibrillation.

Seventeen mongrel dogs, implanted with a pacemaker to induce chronic atrial fibrillation via rapid atrial pacing, were scanned multiple times for a total of 46 CMR scans at 3T. These dogs with different disease durations (0–22 months) were part of a separate longitudinal study aimed at studying the relationship between AF and patho-physiology. In each animal, we measured native and post-contrast $T_1$s and hematocrit. Temporal changes in post-contrast myocardial $T_1$ and ECV, as well as other CMR parameters, were modeled with linear mixed effect models to account for repeated measurements over disease duration.

In 17 animals, post-contrast myocardial $T_1$ decreased significantly from 872 to 698 ms ($p< 0.001$), which corresponds to a 24.9% relative reduction. In contrast, ECV increased from 21.0 to 22.0%

Please send correspondence to: Daniel Kim, The University of Utah, 729 Arapeen Drive, Salt Lake City, Utah 84108, Phone: (801) 587-3861, Fax: (801) 585-3592, Daniel.Kim@hsc.utah.edu.
*M. Koopmann and K. Hong contributed equally as co-first authors

The authors have no conflict of interest related to this work.

(p=0.38), which corresponds to only a 4.5% relative increase. To partially investigate this discrepancy, we quantified collagen volume fraction (CVF) in post-mortem heart tissues of 6 canines sacrificed at different disease duration (0–22 months). CVF quantified by histology increased from 0.9 to 1.9% (p=0.56), which agrees more with ECV than post-contrast myocardial $T_1$. This study shows that post-contrast myocardial $T_1$ and ECV may disagree in a longitudinal canine study. A more comprehensive study, including histologic, cardiac, and renal functional analyses, is warranted to test rigorously which CMR parameter (ECV or post-contrast myocardial $T_1$) agrees more with CVF.

### Keywords

Diffuse myocardial fibrosis; post-contrast myocardial $T_1$; extracellular volume fraction; MRI; heart failure; atrial fibrillation; collagen volume fraction

## Introduction

Diffuse myocardial fibrosis is a well-established marker of adverse structural remodeling in a variety of heart diseases, including: atrial fibrillation (AF) (1), heart failure (2), hypertrophic cardiomyopathy (3,4), aortic stenosis (3,4), cardiac amyloidosis (3,4), myocardial infarction (4), diabetes (5), and congenital heart disease (6). Cardiovascular magnetic resonance (CMR) methods such as post-contrast cardiac $T_1$ mapping (7–9) and extracellular volume (ECV) mapping (4,9–12), derived from native and post-contrast myocardial and blood $T_1$ measurements, are the only validated non-invasive tests for interstitial fibrosis. The CMR field is recognizing that post-contrast myocardial $T_1$ measurement is sensitive to a variety of confounders, including: renal function, hematocrit, magnetic field strength, contrast agent type and dosage, and specific delayed imaging time after administration of contrast agent. To account for these confounders, many investigators in the CMR field are migrating toward myocardial ECV as a marker of diffuse myocardial fibrosis (4,6,10–13). Despite the theoretical advantages of ECV over post-contrast myocardial $T_1$ (14), systematic experimental studies comparing the two measurements are largely lacking, particularly in a longitudinal setting.

Animal models provide a unique opportunity to perform a longitudinal study to monitor the temporal changes in left ventricular (LV) structural remodeling. We have established a canine model with chronic AF to study the relationship between AF and cardiac pathophysiology (15). We sought to leverage this longitudinal canine study and compare the changes in post-contrast myocardial $T_1$ and ECV measurements over disease duration.

## Materials and Methods

### Animal Preparation for CMR at 3T

Seventeen mongrel dogs (12 females, 5 males; mean initial weight = 26 ± 4 kg) with different durations of AF induced by rapid atrial pacing (RAP) (15,16) were included in this study. These canines with chronic AF were part of a separate longitudinal study aimed at characterizing the relationship between AF and cardiac pathophysiology. For more details

on the pacemaker implantation and other procedures conducted to induce AF, see reference (15). In this study, disease duration is defined as the duration since the onset of RAP, since this is the starting point at which cardiac physiology is altered.

As summarized in Table 1, 17 dogs exhibiting different disease durations (0–22 months; mean RAP = 205.8 ± 187 days) were included in this study, for a total of 46 CMR sessions. Canines were fasted for a minimum of 12 hours before MRI. Animals were anesthetized with propofol (5–8 mg/kg, IV) for intubation and subsequently ventilated and maintained in a surgical plane of anesthesia with 1.5–3% isoflurane. Ventilation was controlled using a ventilator (DRE Premier XP MRI-Compatible Veterinary Anesthesia Machine, DRE Veterinary, Louisville, KY). Breath-hold MRI acquisition was performed with the ventilation suspended. Each animal was electrically cardioverted approximately 30 min prior to MRI setup. Note that cardiac $T_1$ mapping and cine MRI methods were performed at least 1 hour after cardioversion to minimize the effects of myocardial stunning. Heart rate, core body temperature, blood pressure, end-tidal $CO_2$, and oxygen saturation were continuously monitored and maintained within normal ranges. Blood was drawn during the MRI exam for hematocrit calculation. Pacemaker implantation and imaging (see below) were performed in accordance with protocols approved by the Institutional Animal Care and Use Committee at the University of Utah.

## CMR Hardware

CMR was performed on two 3T whole-body MRI scanners (Tim Trio and Verio, Siemens Healthcare, Erlangen, Germany) equipped with a gradient system capable of achieving a maximum gradient strength of 45 mT/m and a slew rate of 200 T/m/s. Among a total of 46 CMR scans, 32 and 14 scans were conducted on the Verio and Tim Trio scanners, respectively. The radio-frequency excitation was performed using the body coil. For the experiments conducted on the Tim Trio system, a 6-element body matrix coil array and a spine coil array (with 6 coil elements) were employed for signal reception. For the experiments conducted on the Verio system, a 32-element cardiac coil (RAPID MR International, Columbus, OH) was used for signal reception.

## CMR Protocol

For cardiac $T_1$ measurements, we used the arrhythmia-insensitive rapid (AIR) cardiac $T_1$ mapping pulse sequence (17). Briefly, the AIR cardiac $T_1$ mapping pulse sequence acquires two single-shot balanced steady-state of free precession (b-SSFP) images: 1) a proton density-weighted image and 2) a $T_1$-weighted image. For more details on the AIR cardiac $T_1$ mapping pulse sequence, see reference (17). To minimize the impact of variation in contrast agent dosage and specific delayed imaging time, we measured the weight of each animal immediately prior to MRI, administered exactly 0.15 mmol/kg of gadobenate dimeglumine (Gd-BOPTA) (MultiHance, Bracco Diagnostics Inc., Princeton, NJ), and performed cardiac $T_1$ mapping pre-contrast and at exactly 15 min following Gd-BOPTA administration. We assumed that 15 min after bolus injection of Gd-BOPTA is equilibrium (4,18).

The AIR cardiac $T_1$ mapping pulse sequence was performed with the following imaging parameters: field of view = 260 mm × 195 mm, slice thickness = 8 mm, image acquisition

matrix = 192 × 144, generalized autocalibrating partially parallel acquisitions (GRAPPA) (19) acceleration factor 1.8, flip angle = 35°, saturation-recovery time delay (TD) = 600 ms, receiver bandwidth = 930 Hz/pixel, and temporal resolution = 217 ms. In this study, we also used "paired" consecutive phase-encoding steps in centric k-space ordering to minimize b-SSFP image artifacts due to eddy currents (20). We acquired 3 short-axis slices (base, mid-ventricular, apex) in a single breath-hold duration of 6–9 heart beats (depending on heart rate). Using cardiac long-axis views as guides, for each CMR session, we defined the mid-ventricular short-axis plane as the mid-point between the mitral valve plane and apical cap, the basal short-axis plane as the mid-point between the mid-ventricular plane and mitral valve plane, and the apical short-axis plane as the mid-point between the mid-ventricular plane and apical cap.

As a secondary analysis, we also quantified LV functional parameters from retrospective ECG-gated breath-hold cine MR data acquired with b-SSFP readout (21,22). We imaged the whole heart with a stack of short-axis planes with the following imaging parameters: field of view = 260 mm × 195 mm, image acquisition matrix = 192 × 144, GRAPPA parallel imaging acceleration factor = 1.8, slice thickness = 7 mm, flip angle = 40–45°, receiver bandwidth = 1000 Hz/pixel, echo time (TE) = 1.3 ms, repetition time (TR) = 3 ms, 12–14 short-axis slices (with zero gap), spatial resolution = 1.4 mm × 1.4 mm, number of k-space lines per cardiac phase = 7, temporal resolution = 21 ms, and reconstructed cardiac frames = 25.

### CMR Image Analysis

For cardiac $T_1$ quantification, we calculated the pixel-by-pixel $T_1$ map by dividing the $T_1$-weighted image, $I_{T1W}$, by the proton-density-weighted image, $I_{PD}$, to correct for the unknown equilibrium magnetization, $M_0$, and then solving the Bloch equation governing $T_1$ relaxation describing the ideal saturation-recovery experiment (17):

$$\frac{I_{T1w}}{I_{PD}}=\frac{M_0(1-e^{-TD/T_1})}{M_0}=(1-e^{-TD/T_1}),\ T_1=\frac{-TD}{\mathrm{In}(1-\frac{I_{T1w}}{I_{PD}})}$$

Customized software in MATLAB was used to manually segment the myocardial contours and LV blood pool for each image (i.e., independent contour tracings for native and post-contrast $T_1$ maps per imaging plane per animal per CMR session). Care was taken to avoid partial volume averaging for each contour tracing. AIR cardiac $T_1$ data were randomized for analysis by the first reader (KH), who was blinded to the cine MR and histology results. Myocardial and blood $T_1$s were averaged within their respective contours for each of three LV locations (base, mid, apex). Myocardial ECV was calculated according to (13): (1−hematocrit) × ($\Delta R_{1,m}/\Delta R_{1,b}$) × 100%, where $R_{1,m}$ is $T_1^{-1}$ of myocardium, and $R_{1,b}$ is $T_1^{-1}$ of blood, and is Δ the difference between post-contrast and native.

For cardiac functional assessment, short-axis cine MR images were analyzed using Argus software (Siemens Healthcare, Erlangen, Germany). Another reader (MK), who was blinded to the $T_1$ and histology results, manually segmented the endocardial and epicardial LV contours in end-diastole and end-systole to calculate the following LV functional

parameters: end diastolic volume (EDV), end systolic volume (ESV), stroke volume (SV), LV ejection fraction (LVEF), and LV mass. We note that papillary muscle was excluded for volume measurements, whereas it was included for mass measurement. The interventricular septum was included as part of the LV, while the left ventricular outflow tract was excluded.

## Histological Analysis

Six canines enrolled in this study were terminated at their scheduled disease duration (0, 164, 435, 478, 686, and 690 days since the onset of RAP). Post-mortem tissue specimens (approximately 1 cm × 1 cm × 1 cm in size) were extracted from mid-ventricle of the antero-lateral LV wall of excised hearts fixed in 10% buffered formalin. Tissues were processed according to standard pathology protocol (i.e., tissues fixed in formalin, embedded in paraffin blocks, and sectioned at 4–6 μm). On average, a total of 6–10 sections were prepared with Masson's Trichrome stain to quantify collagen volume fraction (CVF). In a consensus fashion, light-microscopic examination was performed by two experienced pathologists (ECH, RL), who were blinded to animal history, disease duration, and CMR results. The optimal histologic areas were identified visually by consensus, and the resulting digital images were captured using Infinity 2 microscope digital camera (Lumenera, Ottawa, Ontario, Canada) at 100× magnification. Each digital image was evaluated for CVF quantification using customized segmentation software. This software requires user input to learn the patterns, intensity, and color for inclusion (myocytes and interstitial fibrosis) and exclusion (red blood cells, blood vessels, and adipose tissue) elements. We used several training slides of LV tissues with Masson's Trichrome stain to establish the inclusion and exclusion classification criteria. After training, the software generates automatically a classification mask by detecting fibrosis and myocyte pixels based on the trained inclusion and exclusion classification criteria. The two pathologists then compared the resulting classification mask to the original digital Trichrome image, in order to visually confirm the accuracy of the software in identifying the appropriate elements. Finally, using the resulting classification mask (see Figure 2), CVF was calculated as the pixel count of fibrosis (blue) divided by that of myocytes (red).

## Statistical Analysis

For statistical analysis of temporal changes in CMR parameters, we examined the association between the repeated measurements of these parameters and disease duration using a linear-mixed-effect model (LMEM) (23) (N = 46). The exchangeable correlation structure was used to specify the correlation structure among the repeated measurements within each animal. This longitudinal study has an unbalanced distribution of repeated measurements for the different animals. We resolved this issue with LMEM, where the repeated measurements within each animal are treated as a cluster of observations. All LMEMs were fitted with the random intercept for each animal and disease duration as the fixed effect, where p value $< 0.05$ was considered significant. Individual trajectories of CMR parameters were plotted over disease duration. For the temporal change analysis, myocardial and blood T1 values were averaged over the basal and mid-ventricular short-axis planes. Apical short-axis plane results were excluded for the temporal change analysis, because they may be susceptible to partial volume averaging effects. We note that animals

with only one data point (dogs 5, 9, 11, 13, 14, 16, 17) were excluded for the temporal change analysis (but included for other analyses).

For statistical analysis of post-mortem LV tissues, we examined the association between histologic quantification of CVF and disease duration using linear regression (N = 6), where p value < 0.05 was considered significant.

We also performed the following secondary analyses. To investigate whether there are regional differences in $T_1$ measurements between 3 different short-axis planes, we performed analysis of variance (ANOVA) for native myocardial $T_1$, native blood $T_1$, post-contrast myocardial $T_1$, and post-contrast blood $T_1$ measurements. To investigate whether the two different 3T MRI scanners produce different $T_1$ results, we performed a two-sample t-test (two-tailed) for native myocardial and blood $T_1$ measurements only, since the native $T_1$ measurements did not change significantly over disease duration and allows a comparison across different animals (see Table 2). To investigate whether electrical cardioversion induces myocardial edema, in 5 animals, we performed native $T_1$ mapping before and 1 hour after cardioversion and compared their native $T_1$ measurements. A paired t-test (two-tailed) was used to compare native myocardial $T_1$ between pre and post-cardioversion (N = 5), where p value < 0.05 was considered significant.

## Results

Figure 1 shows representative cardiac $T_1$ maps in three short-axis planes of a dog at 464 days since the onset of RAP, illustrating good data and contour tracing quality used in this study. Figure 2 shows post-mortem LV specimens of two different dogs with Masson's trichrome staining at baseline and 22 months after the onset of RAP, as well as their corresponding classification masks used to quantify CVF. These LV specimens and classification masks illustrate good data quality used in this study.

In 17 animals observed over disease duration ranging from 0–22 months (mean RAP = 205.8 ± 187 days), post-contrast myocardial $T_1$ decreased significantly from 872 to 698 ms (Fig. 3; $p < 0.001$), which corresponds to a 24.9% relative reduction. In contrast, ECV increased from 21.0 to 22.0% ($p = 0.38$), which corresponds to only a 4.5% relative increase. This discrepancy was partially investigated by histologic analysis of post-mortem LV tissues. In 6 different dogs sacrificed at different disease duration ranging from 0–22 months, CVF quantified by histology increased from 0.9 to 1.9% (Fig. 3; slope = 0.044, bias = 1.2%, correlation coefficient = 0.30; $p = 0.56$), which agreed more with ECV than post-contrast myocardial $T_1$.

We examined other parameters to identify the cause for this discrepancy. Among cardiac $T_1$ data (native myocardial $T_1$, native blood $T_1$, post-contrast blood $T_1$), only post-contrast blood $T_1$ decreased significantly from 578 to 402 ms (Fig. 3; $p < 0.001$), which corresponds to a 43.8% relative reduction. Note that the temporal trends in post-contrast myocardial and blood $T_1$s are similar. Both native myocardial $T_1$ and native blood $T_1$ did not change significantly (Table 2). Among LV functional parameters (EDV, ESV, SV, LVEF, and LV mass), only LVEF decreased significantly from 46.1 to 33.6% ($p = 0.02$; Table 2), which

corresponds to a 37.2% relative reduction, suggesting progressively worsening LV dysfunction.

The results from the secondary analyses (regional variations in $T_1$, inter-scanner variability of native $T_1$, comparison of native myocardial $T_1$ between pre and post-cardioversion) were as follows. In all animals, the mean native cardiac $T_1$, native blood $T_1$, post-contrast cardiac $T_1$, and post-contrast blood $T_1$ values were not different between basal, mid-ventricular, and apical short-axis planes (see Table 3 for the statistics). According to a two-sample t-test (two-tailed), only mid-ventricular and basal myocardial $T_1$ measurements were significantly different between two different 3T MRI scanners ($p < 0.05$; see Table 4), but note that the magnitude of the percent change was less than 4% for each parameter (i.e., negligible). In 5 animals, the mean native myocardial $T_1$ before (1374 ± 34 ms) and 1 hour after cardioversion (1399 ± 27 ms) was not different ($p = 0.36$), which corresponds to only a 1.8% relative increase.

## Discussion

In this study, in canine models with chronic AF (0 – 22 months), we measured the temporal changes in post-contrast myocardial $T_1$ and myocardial ECV, both of which have been associated with interstitial fibrosis (4,7–12). In the observed canines, post-contrast myocardial $T_1$ decreased significantly over disease duration, whereas myocardial ECV did not. Histologic quantification of CVF in a subset of animals suggests a non-significant difference in CVF over disease duration, which agrees more with ECV than post-contrast myocardial $T_1$. We note that a more comprehensive study, including histologic, cardiac, and renal functional analyses, is warranted to test rigorously which CMR parameter (ECV or post-contrast myocardial $T_1$) agrees more with CVF. Interestingly, post-contrast blood $T_1$ decreased significantly over disease duration, suggesting that decreasing post-contrast myocardial $T_1$ may have been largely driven by decreasing post-contrast blood $T_1$. This observational study is the first report of conflicting findings between post-contrast myocardial $T_1$ and ECV in the context of a longitudinal study. The results of this study agrees with a prior cross-sectional study (9), which first reported a weak association between post-contrast myocardial $T_1$ and ECV in a sub-analysis.

This study also highlights the benefits of myocardial ECV over post-contrast myocardial $T_1$. In the 17 animals studied over disease duration ranging from 0–22 months with an identical AIR cardiac $T_1$ mapping protocol (MRI at exactly 15 min after administration of 0.15 mmol/kg of MultiHance), we observed decreasing trends in post-contrast myocardial $T_1$ and post-contrast blood $T_1$. These temporal trends suggest that decreasing post-contrast myocardial $T_1$ may have been largely driven by decreasing post-contrast blood $T_1$. Our cine MRI data showed that LVEF decreased significantly with disease duration, and it is plausible that a reduced cardiac output could lead to higher concentration of contrast agent in the blood at 15 min after administration (i.e., since less blood is delivered to the kidney per unit time). We note that the separate longitudinal study design did not anticipate renal function to be influenced by chronic AF. Unfortunately, due to the nature of this study (retrospective analysis of data collected from a separate longitudinal study), we are unable to measure changes in renal function over disease duration. Consequently, we are unable to

draw a conclusion on what caused the decreasing trend in post-contrast blood $T_1$ over disease duration. Despite the lack of renal functional data and limited histologic data, our study suggests that CVF agrees better with ECV than post-contrast myocardial $T_1$.

It should be noted that canine $T_1$ measurements reported in this pre-clinical study may not be translatable to other pre-clinical studies using different CMR protocols. A variety of factors, such as field strength, contrast agent type and dosage, specific delayed imaging time, pulse sequence type, heart rate and rhythm, may influence the accuracy of $T_1$ measurements. Therefore, CMR researchers must be careful when translating $T_1$ values presented in this preclinical study into their own studies.

## Study Limitations

A limitation of this study is that the enrolled canines were part of a separate longitudinal study. Consequently, our animal data had an unbalanced distribution of repeated measurements (see Table 1). We used LMEM to account for the unbalanced distribution of repeated measurements. Another limitation of this study is that the histologic analysis was performed for only 6 animals (N=6), which were sacrificed according to the study objectives of the separate longitudinal study. In addition, for each animal, we analyzed a post-mortem tissue specimen of approximately 1 cm × 1 cm × 1 cm in size from the mid-ventricle of the antero-lateral LV wall to represent the whole LV. While it would be more comprehensive to analyze tissues from multiple locations of the LV, this study did not have access to the rest of the heart. A more comprehensive histological evaluation (e.g., biopsy over disease duration) is warranted to confirm our CMR findings. However, we note that performing longitudinal biopsies would add considerable expense and procedural risk to the separate longitudinal study. Furthermore, biopsy samples of the right ventricular septum are small in size (~1–2 mm in length), thereby harder to process and sensitive to sampling errors. Another potential confounder is heart-rate variation in animals under anesthesia during MRI. We typically maintain a steady level of isoflurane during MRI, but the animals' heart rate varies within and across MRI sessions. Consequently, cardiac functional parameters may have been affected by variations in heart rate. Although we performed cine CMR at least one hour after cardioversion, cardiac functional parameters reported in this study may have been influenced by residual myocardial stunning.

## Conclusions

This study shows that post-contrast myocardial $T_1$ and ECV may disagree in a longitudinal canine study. A more comprehensive study, including histologic, cardiac, and renal functional analyses, is warranted to test rigorously which CMR parameter (ECV or post-contrast myocardial $T_1$) agrees more with CVF.

## Acknowledgments

The authors are grateful for funding support from the NIH (HL116895-01A1) and Ben B. and Iris M. Margolis Foundation to Daniel Kim and the German Heart Foundation (Deutsche Herzstiftung e.V.) to Matthias Koopmann.

## List of Abbreviations

| | |
|---|---|
| **LV** | left ventricle |
| **LVEF** | left ventricular ejection fraction |
| **ECV** | extracellular volume |
| **CMR** | cardiovascular magnetic resonance |
| **RAP** | rapid atrial pacing |
| **ECG** | electrocardiogram |
| **b-SSFP** | balanced steady state of free precession |
| **AF** | atrial fibrillation |
| **R** | acceleration rate |
| **bpm** | beats per minute |
| **GRAPPA** | generalized autocalibrating partially parallel acquisitions |
| **$T_1$** | longitudinal relaxation time |
| **LGE** | late gadolinium enhanced |
| **TE** | echo time |
| **TR** | repetition time |
| **AIR** | arrhythmia-insensitive-rapid |
| **Gd-BOPTA** | gadobenate dimeglumine |
| **TD** | saturation-recovery time delay |
| **LMEM** | linear-mixed-effect model |
| **ANOVA** | analysis of variance |
| **EDV** | end diastolic volume |
| **ESV** | end systolic volume |
| **SV** | stroke volume |
| **CVF** | collagen volume fraction |

## References

1. Ling LH, Kistler PM, Ellims AH, Iles LM, Lee G, Hughes GL, Kalman JM, Kaye DM, Taylor AJ. Diffuse ventricular fibrosis in atrial fibrillation: noninvasive evaluation and relationships with aging and systolic dysfunction. J Am Coll Cardiol. 2012; 60(23):2402–2408. [PubMed: 23141493]
2. de Leeuw N, Ruiter DJ, Balk AH, de Jonge N, Melchers WJ, Galama JM. Histopathologic findings in explanted heart tissue from patients with end-stage idiopathic dilated cardiomyopathy. Transplant international : official journal of the European Society for Organ Transplantation. 2001; 14(5):299–306. [PubMed: 11692213]
3. Fontana M, White SK, Banypersad SM, Sado DM, Maestrini V, Flett AS, Piechnik SK, Neubauer S, Roberts N, Moon JC. Comparison of T1 mapping techniques for ECV quantification. Histological validation and reproducibility of ShMOLLI versus multibreath-hold T1 quantification equilibrium

contrast CMR. Journal of cardiovascular magnetic resonance : official journal of the Society for Cardiovascular Magnetic Resonance. 2012; 14:88. [PubMed: 23272651]

4. White SK, Sado DM, Fontana M, Banypersad SM, Maestrini V, Flett AS, Piechnik SK, Robson MD, Hausenloy DJ, Sheikh AM, Hawkins PN, Moon JC. T1 mapping for myocardial extracellular volume measurement by CMR: bolus only versus primed infusion technique. JACC Cardiovascular imaging. 2013; 6(9):955–962. [PubMed: 23582361]
5. Wong TC, Piehler KM, Kang IA, Kadakkal A, Kellman P, Schwartzman DS, Mulukutla SR, Simon MA, Shroff SG, Kuller LH, Schelbert EB. Myocardial extracellular volume fraction quantified by cardiovascular magnetic resonance is increased in diabetes and associated with mortality and incident heart failure admission. European heart journal. 2013
6. Broberg CS, Chugh SS, Conklin C, Sahn DJ, Jerosch-Herold M. Quantification of diffuse myocardial fibrosis and its association with myocardial dysfunction in congenital heart disease. Circulation Cardiovascular imaging. 2010; 3(6):727–734. [PubMed: 20855860]
7. Iles L, Pfluger H, Phrommintikul A, Cherayath J, Aksit P, Gupta SN, Kaye DM, Taylor AJ. Evaluation of diffuse myocardial fibrosis in heart failure with cardiac magnetic resonance contrast-enhanced T1 mapping. J Am Coll Cardiol. 2008; 52(19):1574–1580. [PubMed: 19007595]
8. Sibley CT, Noureldin RA, Gai N, Nacif MS, Liu S, Turkbey EB, Mudd JO, van der Geest RJ, Lima JA, Halushka MK, Bluemke DA. T1 Mapping in Cardiomyopathy at Cardiac MR: Comparison with Endomyocardial Biopsy. Radiology. 2012; 265(3):724–732. [PubMed: 23091172]
9. Miller CA, Naish JH, Bishop P, Coutts G, Clark D, Zhao S, Ray SG, Yonan N, Williams SG, Flett AS, Moon JC, Greiser A, Parker GJ, Schmitt M. Comprehensive validation of cardiovascular magnetic resonance techniques for the assessment of myocardial extracellular volume. Circulation Cardiovascular imaging. 2013; 6(3):373–383. [PubMed: 23553570]
10. Flett AS, Hayward MP, Ashworth MT, Hansen MS, Taylor AM, Elliott PM, McGregor C, Moon JC. Equilibrium contrast cardiovascular magnetic resonance for the measurement of diffuse myocardial fibrosis: preliminary validation in humans. Circulation. 2010; 122(2):138–144. [PubMed: 20585010]
11. Kehr E, Sono M, Chugh SS, Jerosch-Herold M. Gadolinium-enhanced magnetic resonance imaging for detection and quantification of fibrosis in human myocardium in vitro. Int J Cardiovasc Imaging. 2008; 24(1):61–68. [PubMed: 17429755]
12. Jerosch-Herold M, Sheridan DC, Kushner JD, Nauman D, Burgess D, Dutton D, Alharethi R, Li D, Hershberger RE. Cardiac magnetic resonance imaging of myocardial contrast uptake and blood flow in patients affected with idiopathic or familial dilated cardiomyopathy. Am J Physiol Heart Circ Physiol. 2008; 295(3):H1234–H1242. [PubMed: 18660445]
13. Arheden H, Saeed M, Higgins CB, Gao DW, Bremerich J, Wyttenbach R, Dae MW, Wendland MF. Measurement of the distribution volume of gadopentetate dimeglumine at echo-planar MR imaging to quantify myocardial infarction: comparison with 99mTc-DTPA autoradiography in rats. Radiology. 1999; 211(3):698–708. [PubMed: 10352594]
14. Moon JC, Messroghli DR, Kellman P, Piechnik SK, Robson MD, Ugander M, Gatehouse PD, Arai AE, Friedrich MG, Neubauer S, Schulz-Menger J, Schelbert EB. Myocardial T1 mapping and extracellular volume quantification: a Society for Cardiovascular Magnetic Resonance (SCMR) and CMR Working Group of the European Society of Cardiology consensus statement. Journal of cardiovascular magnetic resonance : official journal of the Society for Cardiovascular Magnetic Resonance. 2013; 15:92. [PubMed: 24124732]
15. Dosdall DJ, Ranjan R, Higuchi K, Kholmovski EG, Angel N, Li L, Macleod R, Norlund L, Olsen A, Davies CJ, Marrouche NF. Chronic Atrial Fibrillation Causes Left Ventricular Dysfunction in Dogs but not Goats: Experience with Dogs, Goats, and Pigs. Am J Physiol Heart Circ Physiol. 2013
16. Nishida K, Michael G, Dobrev D, Nattel S. Animal models for atrial fibrillation: clinical insights and scientific opportunities. Europace. 2010; 12(2):160–172. [PubMed: 19875395]
17. Fitts M, Breton E, Kholmovski E, Dosdall D, Vijayakumar S, Hong K, Ranjan R, Marrouche N, Axel L, Kim D. Arrythmia insensitive rapid cardiac T1 mapping pulse sequence. Magnetic Resonance in Medicine. 2013; 70:1274–1282. [PubMed: 23280998]
18. Schelbert EB, Testa SM, Meier CG, Ceyrolles WJ, Levenson JE, Blair AJ, Kellman P, Jones BL, Ludwig DR, Schwartzman D, Shroff SG, Wong TC. Myocardial extravascular extracellular

volume fraction measurement by gadolinium cardiovascular magnetic resonance in humans: slow infusion versus bolus. Journal of cardiovascular magnetic resonance : official journal of the Society for Cardiovascular Magnetic Resonance. 2011; 13:16. [PubMed: 21375743]

19. Griswold MA, Jakob PM, Heidemann RM, Nittka M, Jellus V, Wang J, Kiefer B, Haase A. Generalized autocalibrating partially parallel acquisitions (GRAPPA). Magnetic resonance in medicine : official journal of the Society of Magnetic Resonance in Medicine / Society of Magnetic Resonance in Medicine. 2002; 47(6):1202–1210.
20. Bieri O, Markl M, Scheffler K. Analysis and compensation of eddy currents in balanced SSFP. Magn Reson Med. 2005; 54(1):129–137. [PubMed: 15968648]
21. Carr JC, Simonetti O, Bundy J, Li D, Pereles S, Finn JP. Cine MR angiography of the heart with segmented true fast imaging with steady-state precession. Radiology. 2001; 219(3):828–834. [PubMed: 11376278]
22. Barkhausen J, Goyen M, Ruhm SG, Eggebrecht H, Debatin JF, Ladd ME. Assessment of ventricular function with single breath-hold real-time steady-state free precession cine MR imaging. AJR Am J Roentgenol. 2002; 178(3):731–735. [PubMed: 11856708]
23. Diggle, P.; Diggle, P. Analysis of longitudinal data. Oxford ; New York: Oxford University Press; 2002. p. xvp. 379

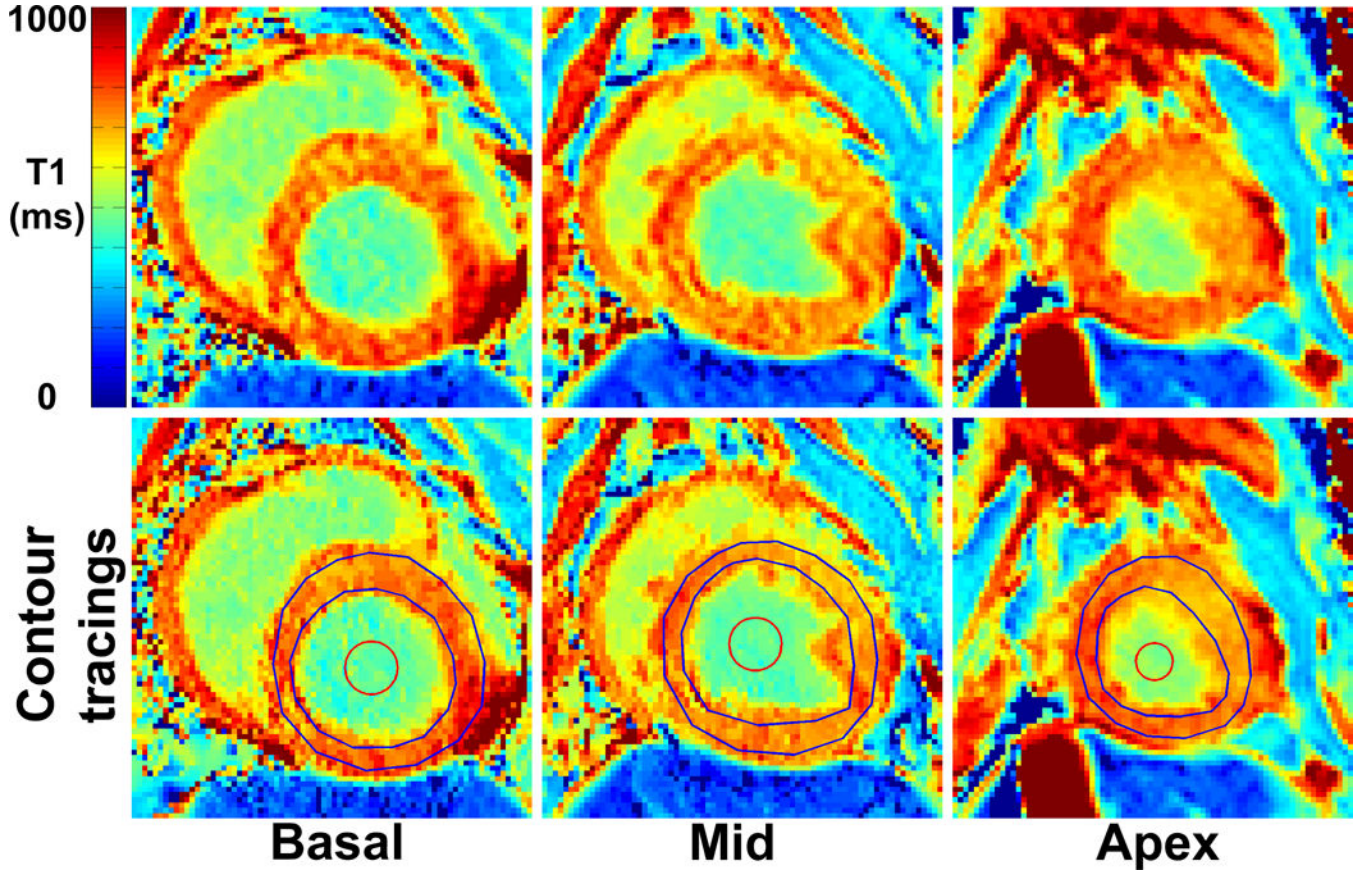


**Figure 1.**

Representative post-contrast cardiac $T_1$ maps (top row) and the same maps with contour tracings (bottom row), illustrating good data and contour tracing quality used in this study: basal (left), mid-ventricular (middle), and apical (right) planes.

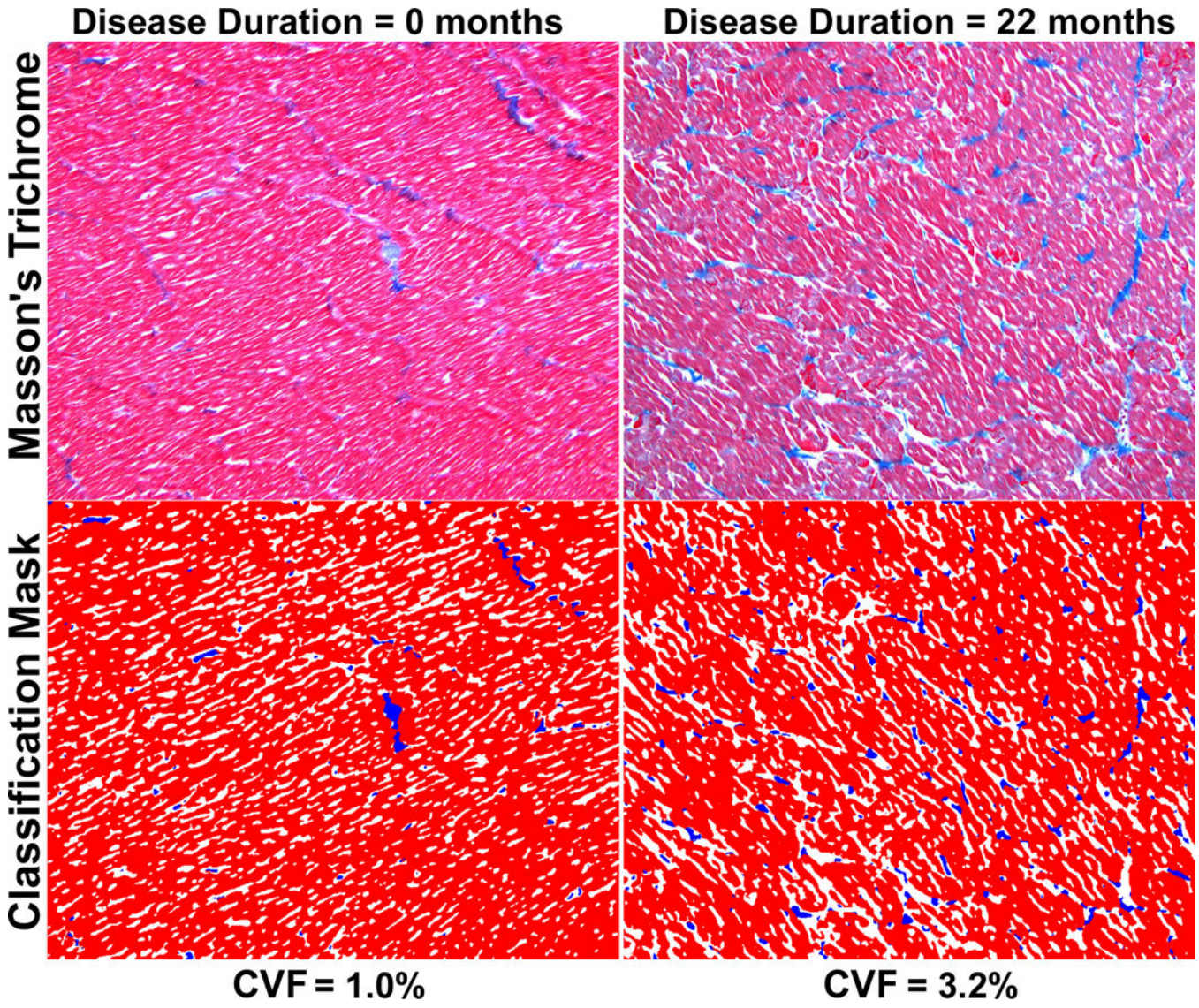


**Figure 2.**

Post-mortem LV samples with Masson's trichrome stain (top row) and the resulting classification masks (bottom row) used to calculate CVF: RAP = 0 (left) and RAP = 22 months (right). All specimens displayed with 100× magnification. Red: myocyte; blue: interstitial fibrosis; white: interstitium (and additional artificial space introduced during histologic slide preparation).

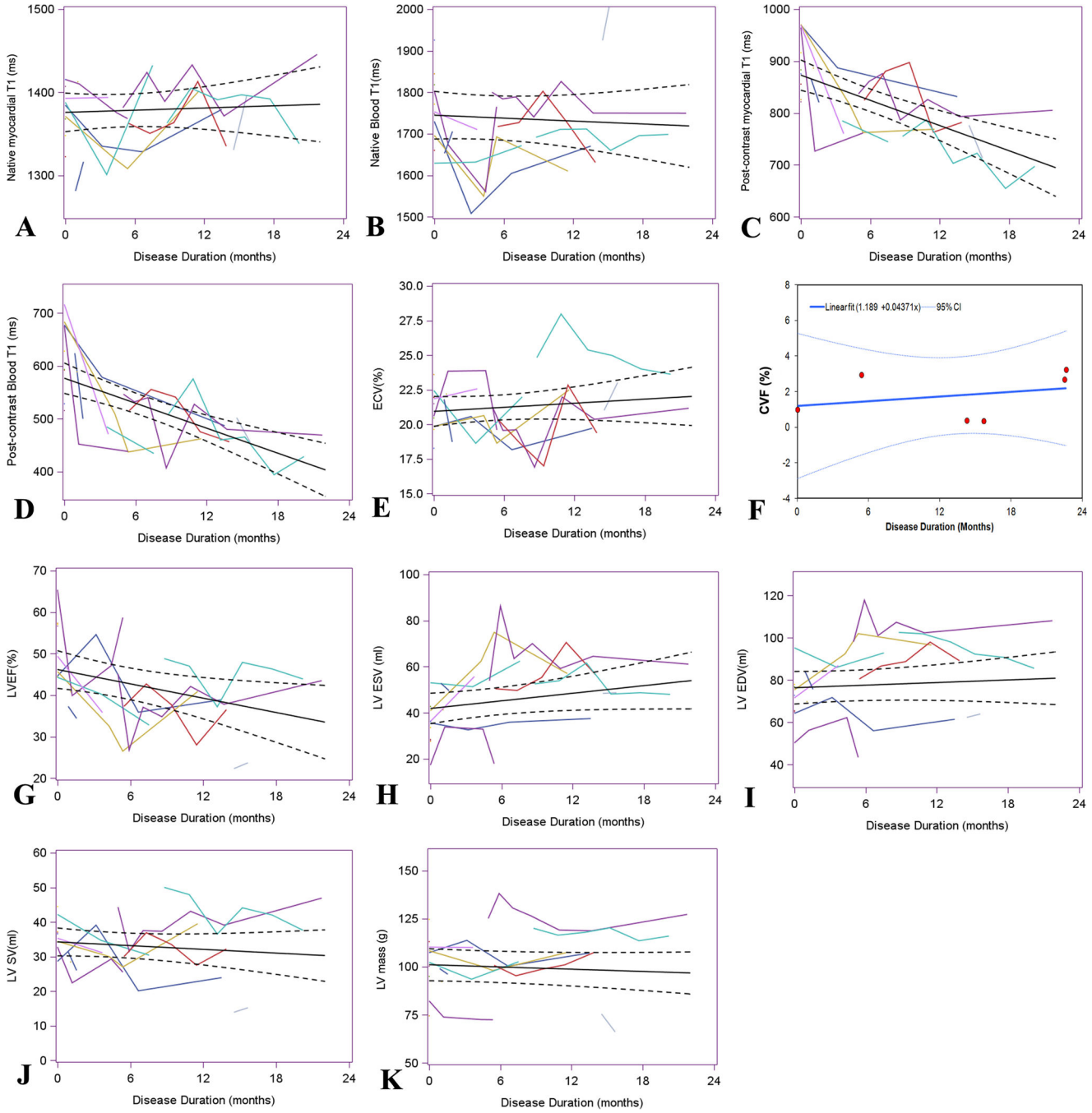


**Figure 3.**

Plot of the estimated regression line (solid line), along with the 95% confidence intervals (dashed lines), describing the temporal changes in the following parameters: native myocardial T1 (a), native blood T1 (b), post-contrast myocardial $T_1$ (c), post-contrast blood $T_1$ (d), ECV (e), and histologic quantification of CVF (f), LVEF (g), ESV (h), EDV (i), SV (j), LV mass (k). For the statistics, see Table 3.

## Table 1

Summary of animal gender, initial weight, and MRI date with respect to days since RAP. 0 day corresponds to before inducing RAP. Mean RAP = 205.8 ± 187 days.

| Canine Number | Gender | Initial weight (kg) | MRI date, RAP (days) |
|---|---|---|---|
| 1 | F | 24.0 | 443, 478 |
| 2 | M | 32.7 | 268, 331, 401, 464, 539, 616 |
| 3 | M | 30.0 | 152, 180, 215, 262, 334, 418, 663 |
| 4 | M | 31.1 | 167, 223, 286, 349, 423 |
| 5 | F | 26.0 | 33 |
| 6 | F | 24.0 | 0, 97, 203, 412 |
| 7 | F | 22.7 | 0, 130, 164, 352 |
| 8 | F | 19.0 | 0, 37, 135, 164 |
| 9 | F | 23.0 | 0 |
| 10 | F | 26.9 | 0, 109, 230 |
| 11 | F | 27.2 | 0 |
| 12 | F | 25.2 | 0, 113 |
| 13 | M | 30.8 | 0 |
| 14 | M | 25.2 | 0 |
| 15 | F | 28.2 | 27, 48 |
| 16 | F | 27.1 | 0 |
| 17 | F | 29.0 | 0 |

## Table 2

LMEM statistics to estimate the temporal changes of CMR parameters. We note that the T1 and ECV measurements are averaged over the basal and mid-ventricular short-axis planes. CI: confidence interval; SE: standard error. Mean RAP = 205.8 ± 187 days. For graphical displays of these parameters, see Figure 3. Percent change is defined as 100% × (final-initial)/initial.

| CMR Variable | Estimated change per month (95% CI) | SE | *p*-value | *Percent change* |
|---|---|---|---|---|
| Native myocardial $T_1$ | 0.44(−1.97, 2.86) ms | 1.18 | 0.71 | 0.7 % |
| Native blood $T_1$ | −1.17(−6.04, 3.96) ms | 2.38 | 0.62 | −1.3 % |
| Post-contrast myocardial $T_1$ | −8.11 (−11.31, −4.92) ms | 1.55 | <0.001 | −24.9 % |
| Post-contrast blood $T_1$ | −7.89 (−10.98, −4.79) ms | 1.50 | <0.001 | −43.8 % |
| ECV | 0.049 (−0.064, 0.16) % | 0.06 | 0.38 | 4.5 % |
| EDV | 0.21 (−0.37, 0.78) ml | 0.28 | 0.47 | −37.2 % |
| ESV | 0.55 (−0.08, 1.18) ml | 0.31 | 0.09 | 5.5 % |
| SV | −0.18 (−0.56, 0.20) ml | 0.19 | 0.34 | 22.2 % |
| LVEF | −0.58 (−1.05, −0.10) % | 0.23 | 0.02 | −12.2 % |
| LV Mass | −0.19 (−0.61, 0.22) g | 0.20 | 0.34 | −3.9 % |

## Table 3

Comparison of mean native myocardial $T_1$, native blood $T_1$, post-contrast myocardial $T_1$, and post-contrast blood $T_1$ values for the basal, mid-ventricular, and apical short-axis planes. According to ANOVA, all four $T_1$ measurements were not different among the three short-axis planes. Mean RAP = 205.8 ± 187 days.

| CMR variable | Base | Mid | Apex | *p*-value |
|---|---|---|---|---|
| Native myocardial $T_1$ | 1383 ± 44 ms | 1372 ± 47 ms | 1390 ± 53 ms | 0.19 |
| Native Blood $T_1$ | 1725 ± 105 ms | 1719 ± 104 ms | 1692 ±89 ms | 0.29 |
| Post-contrast myocardial $T_1$ | 831 ± 74 ms | 811 ± 82 ms | 823 ± 81 ms | 0.71 |
| Post-contrast Blood $T_1$ | 527 ± 77 ms | 521 ± 82 ms | 534 ± 80 ms | 0.54 |

## Table 4

Comparison of mean native myocardial and blood $T_1$ values across two different 3T MRI scanners. According to a two-sample t-test (two-tailed), only mid-ventricular and basal myocardial $T_1$ measurements were significantly different ($p < 0.05$), but note that the magnitude of the percent change was less than 4% for each parameter (i.e., negligible). Percent change is defined as 100% × (Trio-Verio)/Verio.

| CMR variable | Verio | Tim Trio | *p*-value | Percent change |
|---|---|---|---|---|
| Native apical myocardial $T_1$ | 1396 ± 57 ms | 1379 ± 42 ms | 0.35 | −1.2 % |
| Native mid-ventricular myocardial $T_1$ | 1386 ± 43 ms | 1340 ± 40 ms | 0.002 | −3.3 % |
| Native basal myocardial $T_1$ | 1399 ± 36 ms | 1348 ± 42 ms | <0.001 | −3.7 % |
| Native apical blood $T_1$ | 1689 ±82 ms | 1700 ± 106 ms | 0.73 | 0.6 % |
| Native mid-ventricular blood $T_1$ | 1728 ± 108 ms | 1700 ± 97 ms | 0.41 | −1.6 % |
| Native basal blood $T_1$ | 1730 ± 109 ms | 1713 ± 100 ms | 0.63 | −1.0 % |